AUTOMATIC 3-D MUSCLE AND FAT SEGMENTATION OF THIGH MAGNETIC RESONANCE IMAGES IN INDIVIDUALS WITH SPINAL CORD INJURY

Samineh Mesbah[1,2,5], Ahmed Shalaby[2], Andrea Willhite[4,5], Susan Harkema[3,4,5], Enrico Rejc[3,4], Ayman El-baz[2]

[1] Department of Electrical and Computer Engineering, University of Louisville, Louisville, KY, USA
[2] Department of Bioengineering, University of Louisville, Louisville, KY, USA
[3] Department of Neurological Surgery, University of Louisville, Louisville, USA
[4] Kentucky Spinal Cord Injury Research Center, University of Louisville, Louisville, Kentucky, USA
[5] Frazier Rehab Institute, Kentucky One Health, Louisville, KY, USA

ABSTRACT

Spinal cord injured (SCI) individuals are often subject to skeletal muscles deterioration and adipose tissue gain in paralyzed muscles. These negative impacts can limit motor functions and lead to secondary complications such as diabetes, cardiovascular diseases and metabolic syndrome. In this study, we proposed an accurate and fast automatic framework for thigh muscle and fat volume segmentation using magnetic resonance 3-D images, which is aimed at quantifying the impact of SCI and different rehabilitative interventions for these individuals. In this framework, the subcutaneous, intermuscular fat volumes were segmented using a Linear Combination of Discrete Gaussians (LCDG) algorithm. In order to segment muscle group volumes, each MRI volume was initially registered to a training database using a 3-D Cubic B-splines based method. As a second step, a 3-D level-set method was developed utilizing the Joint Markov Gibbs Random Field (MGRF) model that integrates first order appearance model of the muscles, spatial information, and shape model to localize the muscle groups. The results of testing the new method on 15 MRI datasets from 10 SCI and 5 non-disabled subjects showed accuracy of 87.10% for fat segmentation and 96.71% for muscle group segmentation based on Dice similarity coefficient measurements.

Index Terms— MRI, Level-set, MGRF, LCDG, SCI

1. INTRODUCTION

Severe spinal cord injury (SCI) leads to a drastic musculoskeletal deterioration [1]. In particular, the muscle paralyzed by an upper motor neuron lesion undergoes severe atrophy and consequent reduction of force generation capability, a gradual transformation to a fast-fatigable phenotype and extensive fatigue. These conditions may limit motor functions even if neuronal control was sufficient. Individuals with severe SCI are also prone to gain adipose tissue at different sites (i.e. subcutaneous, intermuscular fat) [2] [3]. These physiological adaptations can also lead to secondary complications such as higher risk of diabetes, cardiovascular diseases and metabolic syndrome [2]. However, in spite of the above-mentioned deleterious adaptations due to SCI, paralyzed skeletal muscles can be reconditioned by different treatments that include neuromuscular electrical stimulation, dietary programs and assisted movement training [4] [5].

Magnetic resonance imaging (MRI) is a commonly used technique to evaluate the effects of SCI and other conditions that lead to prolonged disuse (i.e., bed rest) or reduced physical activity (i.e., ageing) on skeletal muscle mass and adipose tissue distribution [6] [7]. Three-dimensional MRI scans of thigh muscles have also been collected to monitor the effects of neuromuscular electrical stimulation and other rehabilitative interventions on skeletal muscle in individuals with SCI [8]. In order to properly quantify the impact of different conditions and interventions on skeletal muscle and adipose tissue, the MRI slices need to be segmented based on muscle tissue, subcutaneous fat and intermuscular fat. In addition, it is also important to assess and compare the muscle mass of specific muscle groups (i.e. knee extensors and knee flexors), as the relationship between agonist and antagonist muscles may influence the ability to perform a movement and its characteristics.

The major limitation for assessing these parameters is the fact that the task of segmentation and analysis of MRI slices is currently performed manually by experts. The manual evaluation of each slice in 3-D datasets is laborious and time-consuming; furthermore, it is also subject to inter- and intra-operator variability. These limitations also cause lack of scalability to a higher number of patients and treatment methods. Therefore, reliable and accurate automatic or semi-automatic methods for detecting the volume of different muscle groups as well as intermuscular and subcutaneous fat from MRI images are highly indispensable.

There have been several studies in the literature to automate the segmentation of muscle area and adipose tissue in thigh MRI images. Urricelqui et al. [9] proposed a recursive algorithm to segment the fat and muscle tissues in the thigh images of 30 obese subjects. In this algorithm at each iteration, they divide images into sub-images and model the histogram for each sub-image and find the proper

Fig. 1. The proposed framework for muscles/fat analysis on MRI volumes.

threshold for segmentation. In this work, they did not separate subcutaneous fat from intermuscular fat. Positano et al. [10] used a similar MRI dataset (20 obese individuals) to segment total thigh mask, subcutaneous fat and bone using fuzzy c-mean clustering method and Snake algorithm. They also used EM algorithm to separate intermuscular fat and muscle tissue. Makrogiannis et al. [11] used WS and FS MRIs to segment thigh volumes in an elderly population. Subcutaneous fat was segmented using parametric deformable model and centroid k-means clustering was utilized in the feature domain defined by the voxel intensities for intermuscular fat and muscle tissue. Valentinitsch et al. [12] in 2013 used similar clustering and histogram thresholding to segment soft tissue, muscle and bone in MR images of calves in individuals with type-2 diabetes and thighs of elderly subjects with and without osteoarthrosis. Furthermore, Orgiu et al. [13] used fuzzy c-means algorithm to segment total muscle, fat and bone area in young normal, old normal and old obese population. They separated the subcutaneous from intermuscular fat using morphological-based segmentation technique with an active contour Snake.

All of these studies are focused on segmentation of fat and muscle area using intensity-based methods only. However, no muscle group segmentation was done in these studies. There have been a number of studies done recently on muscle volume segmentation on MR images of thigh muscles. The objectives of these studies were to segment the entire volume of certain muscle groups or each individual muscle in addition to subcutaneous and intermuscular fat segmentation. Andrews and Hamarneh [14] proposed a combination of generalized log-ratio probabilistic shape model and random forest binary detector to segment each individual muscle of the human thigh. Ahmad et al. [15] proposed a semi-automatic framework of atlas construction and image registration to segment the quadriceps muscle group. The used input was used to draw a segmentation border and use that to build the atlas. However, no segmentation of adipose tissue was done in these two studies. Another atlas-based segmentation method was proposed by Troter et al. [16] to segment four individual muscle volumes inside the quadriceps group. They presented a semi-automated single-atlas and fully automated multiple-atlas approaches for the segmentation, suggested that the single-atlas method was more robust for single muscle segmentation and has a better accuracy. However, there is no utilization of any appearance features in their model.

In this work, we propose a probabilistic model that takes into account the information of the image intensity, shape and appearance concurrently to 1) automatically segment MRI volumes of adipose tissue into subcutaneous and intermuscular fat and 2) segment the MRI volumes related to the thigh muscle tissue into three main muscle groups: knee extensors, knee flexors and hip adductor muscles.

Before we start demonstrating the proposed method, we will define some basic terminologies, as in [17]. Let $\mathbf{R} = \{(x,y,z) : 0 \le x \le X-1,\ 0 \le y \le Y-1,\ 0 \le z \le Z-1\}$; $\mathbf{Q} = \{0,1,\ldots,Q-1\}$; and $\mathbf{L} = \{0,1,2,3\}$ denote a finite 3-D arithmetic lattice of the size of XYZ supporting grayscale images and their region (segmentation) maps, a finite set of Q integer gray values, and a set of region labels, respectively. Let $\mathbf{g} = \{g_{x,y,z} : (x,y,z) \in \mathbf{R};\ g_{x,y,z} \in \mathbf{Q}\}$ and $\mathbf{m} = \{m_{x,y,z} : (x,y,z) \in \mathbf{R};\ m_{x,y,z} \in \mathbf{L}\}$ be a grayscale image taking values from $\mathbf{Q}$, i.e., $\mathbf{g} : \mathbf{R} \to \mathbf{Q}$, and a region map taking values from $\mathbf{L}$, i.e., $\mathbf{m} : \mathbf{R} \to \mathbf{L}$, respectively .

2. METHODS

A 3-D level-set-based framework for fat suppressed (FS) and water suppressed (WS) MRI muscles and fat segmentation is proposed in Fig. 1. The proposed system consists of the following three steps: 1) As a preprocessing step, each input FS- and WS-MRI volume is automatically segmented to extract muscle volume from adipose tissue and separate subcutaneous fat area from the intermuscular fat using Linear Combination of Discrete Gaussians (LCDG) algorithm [17]; 2) Each segmented muscle volume and it's manually segmented muscle groups (training dataset) is registered/aligned to a reference dataset using a 3-D cubic B-splines based approach [18] to account for the anatomical differences of each patient's extracted muscle volumes from adipose tissue and bone; and 3) Implementing a Joint Markov Gibbs Random Field (MGRF) model that integrates first order appearance model of the muscles, spatial information, and appearance-based shape model (muscles anatomy) to segment/localize the three muscle groups: knee extensors, knee flexors and hip adductors for the test subjects.

2.1. Joint Markov Gibbs Random Field model

An input MRI data, **g**, registered to a reference database, and its map, **m**, are described with a joint probability model: P(**g**,**m**) = P(**g**|**m**)P(**m**), which combines a conditional distribution of the volume given the map P(**g**|**m**), and an unconditional probability distribution of maps P(**m**) = P_{sp}(**m**)P_V(**m**), as in [19]. Here, P_{sp}(**m**) denotes an adaptive shape prior, and P_V(**m**) is a Gibbs probability distribution with potentials **V**, which specifies an MGRF model of **m**. Details of the model's components are outlined below.

2.1.1 Appearance-based Shape Model:

In order to reduce the variability across subjects and enhance the segmentation accuracy, an adaptive shape model of each muscle group is employed. To create the shape database, a training set of volumes, collected from different subjects, are registered to a reference dataset using a 3-D B-splines based transformation developed in [18]. The probabilistic shape priors are spatially variant independent random fields of region labels, as follows:

$$Psp(\boldsymbol{m}) = \prod p_{sp:x,y,z}(m_{x,y,z}) \quad (1)$$

where $p_{sp:x,y,z}(l)$ is the voxel-wise empirical probabilities for each label $l \in \mathbf{L}$. To segment each input MRI data, an adaptive process guided by the visual appearance features of the input MRI data is used to construct the shape prior. This shape prior consists of four labels: the 3 muscle groups and the background. In the training phase, we use N-1 (N number of subjects) manually segmented data sets by an MRI expert to create the probabilistic maps for the four labels. For the testing phase, each test MRI volume is registered using the same approach in [18], to the training sets used to create the discussed shape prior.

2.1.2. Spatial Interaction Model:

In order to increase the segmentation accuracy, spatially homogeneous 3-D pair-wise interactions between the region labels are additionally incorporated in our model. These interactions are estimated using the Potts model (i.e., an MGRF with the nearest 26-neighbors of the voxels), and analytic bi-valued Gibbs potentials, that depend only on whether the nearest pairs of labels are equal or not. Let f_{eq}(**m**) denote the relative frequency of equal labels in the neighboring voxel pairs. The initial region map results in an approximation with the following analytical maximum likelihood estimates of the potentials [20]:

$$v_{eq} = -v_{ne} \approx 2f_{eq}(\mathbf{m}) - 1 \quad (2)$$

which allows for computing the voxel-wise probabilities $p_{V:x,y,z}(l)$ of each label; $l \in \mathbf{L}$. More details are in [18].

2.1.3 First-Order Appearance (Intensity) Model:

Our approach also accounts for the visual appearance of the muscles besides the learned shape model and the spatial interactions. Hence, for more accurate modeling of the current FS-MRI appearance, we use the linear combination of discrete Gaussians (LCDG) model with positive and negative discrete Gaussian (DG) components. The LCDG separates the mixed empirical 1D distribution of FS-MRI voxel intensities into two distinct components associated with each label [18]. This approximation adapts the segmentation to the changing appearance, such as non-linear intensity variations caused by data acquisition systems. The LCDG models the empirical distribution of the muscles labels more accurately than a conventional mixture of only positive Gaussians. This yields a better initial region map that is formed by the voxel-wise classification of the volume grey values. The LCDG model is described in detail in [17].

2.2 Final segmentation using level-set

As mentioned above, the proposed approach incorporates the adaptive prior shape information to two other features (first order appearance and spatial interactions) into the level-set segmentation, which in turn highlights one of the most important advantages of our framework. These features are estimated directly from the input data to be segmented, making the proposed framework an adaptive approach. These three features are used to provide the voxel-wise guidance of the level-set. For each voxel (x,y,z), the level-set speed function is defined as: $F_n(x,y,z) = \kappa\vartheta(x,y,z)$ where κ is the mean contour curvature and $\vartheta(x,y,z)$ specify the magnitude and direction of contour evolution at the voxel (x,y,z):

$$\vartheta(x,y,z) = \begin{cases} -P_{ob:x,y,z} & if\ P_{ob:x,y,z} > P_{bg:x,y,z} \\ P_{bg:x,y,z} & Otherwise \end{cases} \quad (3)$$

where $P_{ob:x,y,z}$ and $P_{bg:x,y,z}$, are the joint MGRF probabilities for each muscle group and background, respectively. $P_{ob:x,y,z} = \frac{\Omega_{ob:x,y,z}}{\Omega_{ob:x,y,z}+\Omega_{bg:x,y,z}}$ and $P_{bg:x,y,z} = 1 - P_{ob:x,y,z}$; where $\Omega_{ob:x,y,z} = p(q|l)p_{V:x,y,z}(l)p_{sp:x,y,z}(l)$. Here $p(q|l)$ denote the voxel-wise probability of the intensity $q \in \mathbf{Q}$ for the LCDG model of each group (l = 1, 2, 3) or background (l = 0) appearance, $p_{V:x,y,z}(l)$ is the mucle group label probability of **m** in the MGRF spatial model; and $p_{sp:x,y,z}(l)$ is the probability of the muscle group label in the adaptive shape prior P_{sp}(**m**), similar to the method in [21-23].

3. EXPERIMENTAL RESULTS

The 3-D MRI slices were recorded using Siemens 3T Magnetom Skyra with pulse sequence – t1 vibe (for 3-D VIBE images) for in phase, opposite phase, water, and fat imaging. The image dimensions (X, Z, Y) are 320 x 320 x 208 and the series length is 1. Voxel dimensions (X, Z, Y) are 1.5 x 1.5 x 1.5 mm, Size of series point is 0.006 seconds and the slice gap is equal to zero because these are 3-D images. The thigh MRI scans analyzed in this study (N = 15) were collected from 10 individuals with chronic motor complete SCI (age: 31.5 ± 9.2 years; time since injury: 8.0 ± 9.0 years; 7 males and 3 females) and 5 non-disabled subjects (age 28.5 ± 4.1; 3 males and 2 females). The recorded MRI volumes from the SCI subjects were prior to any treatment; 3 of these subjects also underwent MRI scan after intense locomotor training [24]. All participants were fully informed about the aim of the study and have provided their written consents,

which have been approved by the University of Louisville Institutional Review Board.

In this study, the 50 central MRI slices between greater trochanter and lateral epicondyle of the femur were considered for further analysis. All manual segmentations used in training and verifying the segmentation results were created and revised by MRI experts.

To assess the results of the preprocessing step, Fig. 2 shows the LCDG results on the FS- and WS-MRI volumes for extraction of the muscles and segmenting the subcutaneous fat from the intermuscular fat. On the other hand, cross sectional results for the 3-D registration process for different test subjects are shown in Fig. 3.

Sample cross sections of the 3-D segmentations for FS-MRI volumes of different subjects are shown in Fig. 4. The 3-D reconstructions of the three segmented groups for different subjects are presented in Fig. 5. It is clear that our proposed approach is successful in segmenting the main three muscle groups.

To evaluate the accuracy of fat segmentation results, we calculated the percentage of Dice similarity coefficient (DSC) [25] by comparing the results of automatic segmentation to the ground truth for each subject. For evaluating the muscle group segmentation, the model was trained with N-1 subjects and tested on the remaining 1 subject, and repeated of every subject in SCI and non-disabled groups separately. The results were compared to the ground truth using DSC measure. Table 1 summarizes the average segmentation accuracy for each test subject. The proposed method reaches 96.71 ± 1.55% overall DSC for muscle group segmentation, 94.02 ± 2.16% for subcutaneous fat segmentation and 80.19 ± 5.39% for intermuscular fat segmentation.

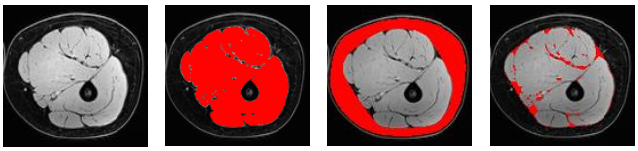

(a) (b) (c) (d)

Fig.2. Examples for the utilization of LCDG to segment the soft tissue: (a) original image; Red area in (b) shows the muscle, in (c) shows the subcutaneous fat, and in (d) shows the intermuscular fat.

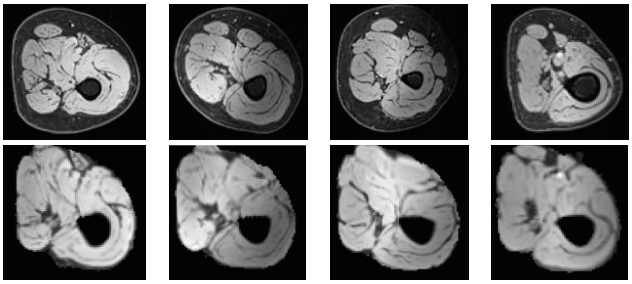

Fig. 3. Examples of registration/alignment results for four subjects using the 3-D spline approach in [18]. First row: the original images before registration; Second row: the images after registering to the reference.

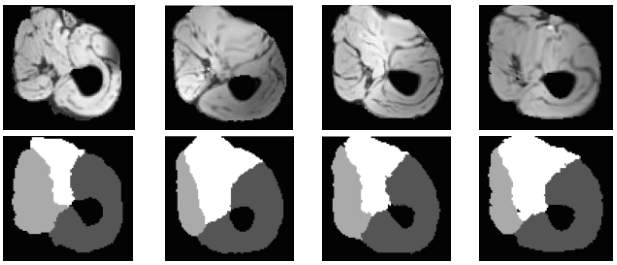

Fig.4. The cross-sectional segmentation results for four subjects using the proposed approach. First row: the original MR images after registration; Second row: the MR images after segmentation.

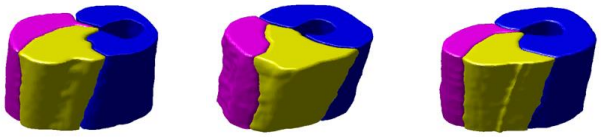

Fig.5. The 3-D reconstruction for 3 different subjects using the proposed segmentation approach.

Table 1: The segmentation accuracy of the proposed approach for 10 SCI and 5 Non-disabled subjects

Subject ID	Dice Similarity (%)				
	Knee extensors	**Knee flexors**	**Adduct muscles**	**Subcutaneous fat**	**Inter/Intra fat**
SCI#1	98.66	96.84	96.68	91.00	72.69
SCI#2	98.71	96.94	96.11	93.57	83.49
SCI#3	98.73	96.91	96.49	93.25	82.34
SCI#4	98.48	96.67	95.75	91.42	81.69
SCI#5	98.29	96.94	96.82	91.53	83.59
SCI#6	98.58	97.46	96.61	95.99	83.51
SCI#7	98.04	96.30	95.53	96.87	83.10
SCI#8	98.24	96.94	95.79	96.99	78.20
SCI#9	98.70	97.22	96.61	94.89	84.40
SCI#10	97.94	96.43	95.63	94.14	67.02
ND#1	97.54	92.90	94.53	94.65	85.84
ND#2	96.27	93.46	97.15	92.61	78.61
ND#3	96.66	91.51	94.33	91.49	85.16
ND#4	98.03	96.25	96.91	94.40	73.30
ND#5	98.65	96.23	96.61	97.54	79.83

*SCI: Spinal Cord Injured
*ND: Non-disabled

4. CONCLUSION

In this study, an automatic framework was proposed to accurately segment thigh muscle groups and fat volumes in healthy and SCI individuals. The high accuracy presented in the results section for muscle group segmentation demonstrates the advantage of incorporating appearance and spatial information into a level-set model for automatic muscle volume segmentation. It is notable that manual segmentation of intermuscular fat areas is a challenging task since it is difficult to mark all the areas with lower intensities, therefore it causes more dissimilarities between manual and automatic method. However, the automatic method can be used for guiding the manual segmentation of the fat area in the future. While the main focus of this study was on SCI subjects, the close accuracy in the non-disabled group supports the claim that our proposed framework has the capacity to be applied in other populations where the segmentation of thigh muscle and fat volumes can be a valuable assessment.

REFERENCES

[1] R. K. Shields and S. Dudley-Javoroski, "Musculoskeletal Plasticity After Acute Spinal Cord Injury: Effects of Long-Term Neuromuscular Electrical Stimulation Training," *J Neurophysiol,* vol. 95, no. 4, p. 2380–2390, 2006.

[2] A. S. Gorgey, D. R. Dolbow, J. D. Dolbow, R. K. Khalil, C. Castillo and D. R. Gater, "Effects of spinal cord injury on body composition and metabolic profile – Part I," *The Journal of Spinal Cord Medicine,* pp. 693-702, 2014.

[3] Deepak Kumar, Dimitrios C. Karampinos, Toran D. MacLeod, Wilson Lin, Lorenzo Nardo, Xiaojuan Li, Thomas M Link, Sharmila Majumdar, Richard B Souza, "Quadriceps intramuscular fat fraction rather than muscle size is associated with knee osteoarthritis," *Osteoarthritis Cartilage,* vol. 22, p. 226–234, 2014.

[4] A. S. Gorgey, D. R. Dolbow, J. D. Dolbow, R. K. Khalil and D. R. Gater, "The effects of electrical stimulation on body composition and metabolic profile after spinal cord injury – Part II," *The Journal of Spinal Cord Medicine,* vol. 38, no. 1, pp. 23-37, 2015.

[5] A. S. Gorgey, D. R. Dolbow, D. X. Cifu and D. R. Gater, "Neuromuscular electrical stimulation attenuates thigh skeletal muscles atrophy but not trunk muscles after spinal cord injury," *Journal of Electromyography and Kinesiology,* p. 977–984, 2013.

[6] C. Elder, D. Apple, C. Bickel, R. Meyer and G. Dudley, "Intramuscular fat and glucose tolerance after spinal cord injury – a cross-sectional study," *Spinal Cord,* p. 711–716, 2004.

[7] R, Pisot; U, Marusic; G, Biolo; S, Mazzucco; S, Lazzer; B, Grassi; C, Reggiani; L, Toniolo; PE, di Prampero; A, Passaro; M, Narici; S, Mohammed; J, Rittweger; M, Gasparini; M, Gabrijelčič Blenkuš; B, Šimunič, "Greater loss in muscle mass and function but smaller metabolic alterations in older compared with younger men following 2 wk of bed rest and recovery.," 2016.

[8] T. E. Ryan, J. T. Brizendine, D. Backus and K. K. McCully, "Electrically Induced Resistance Training in Individuals With Motor Complete Spinal Cord Injury," *Archives of Physical Medicine and Rehabilitation,* vol. 94, pp. 2166-73, 2013.

[9] L. Urricelqui, A. Malanda and A. Villanueva, "Automatic segmentation of thigh magnetic resonance images," *International Journal of Medical, Health, Biomedical, Bioengineering and Pharmaceutical Engineering,* vol. 3, no. 10, pp. 314-320, 2009.

[10] V. Positano, T. Christiansen, M. F. Santarelli, S. Ringgaard, L. Landini and A. Gastaldelli, "Accurate Segmentation of Subcutaneous and Intermuscular Adipose Tissue From MR Images of the Thigh," *J Magn Reson Imaging,* no. 29, p. 677–684, 2009.

[11] S. Makrogiannis, S. Serai, K. W. Fishbein, C. Schreiber, L. Ferrucci and R. G. Spencer, "Automated Quantification of Muscle and Fat in the Thigh from Water-, Fat-and Non-Suppressed MR Images," *J Magn Reson Imaging,* vol. 35, no. 5, p. 1152–1161, 2012.

[12] A. Valentinitsch, D. C. Karampinos, H. Alizai, K. Subburaj, D. Kumar, T. M. Link and S. Majumdar, "Automated unsupervised multi-parametric classification of adipose tissue depots in skeletal muscle," *J Magn Reson Imaging,* vol. 37, no. 4, p. 917–927, 2013.

[13] S. Orgiu, C. L. Lafortuna, F. Rastelli, M. Cadioli, A. Falini and G. Rizzo, "Automatic Muscle and Fat Segmentation in the Thigh From T1-Weighted MRI," *J. MAGN. RESON. IMAGING,* vol. 43, no. 3, pp. 601-10, 2015.

[14] S. Andrews and G. Hamarneh, "The Generalized Log-Ratio Transformation: Learning Shape and Adjacency Priors for Simultaneous Thigh Muscle Segmentation," *IEEE Transactions on Medical Imaging,* vol. 34, no. 9, pp. 1773-1787, 2015.

[15] E. Ahmad, M. H. Yap, H. Degens and J. S. McPhee, "Atlas-registration based image segmentation of MRI human thigh muscle in 3-D space," in *Proceedings of SPIE*, 2014.

[16] A. L. Troter, A. Fouré, M. Guye, S. Confort-Gouny, J. Mattei, J. Gondin, E. Salort-Campana and D. Bendahan, "Volume measurements of individual muscles in human quadriceps femoris using atlas-based segmentation approaches," *J of Magn Reson MAter Phy,* vol. 29, p. 245–257, 2016.

[17] A. Farag, A. El-baz and G. Gimelfarb, "Precise segmentation of multi-modal images," *IEEE Trans. Image Process.,* vol. 15, no. 4, pp. 952-968, 2006.

[18] B. Glocker, A. Sotiras, N. Komodakis and N. Paragois, "Deformable medical image registration: Setting the state of the art with discrete methods," *Annual Review of Biomedical Engineering,* vol. 13, pp. 219-244, 2011.

[19] A. El-Baz, G. Gimel'farb, J. S. Suri, "Stochastic Modeling for Medical Image Analysis", Taylor & Francis, ISBN 9781466599079, January 2016.

[20] F, Khalifa; GM, Beache; G, Gimel'farb; GA, Giridharan; A, El-Baz, "Accurate automatic analysis of cardiac cine images.," *IEEE Trans Biomed Eng,* vol. 59, no. 2, pp. 445-55, 2012.

[21] I. Reda, A. Shalaby, A. El-Baz et al., "Computer-aided diagnostic tool for early detection of prostate cancer," 2016 IEEE International Conference on Image Processing (ICIP), Phoenix, AZ, 2016, pp. 2668-2672.

[22] M. S. Aslan, A. Shalaby and A. A. Farag, "Clinically desired segmentation method for vertebral bodies," 2013 IEEE 10th International Symposium on Biomedical Imaging, San Francisco, CA, 2013, pp. 840-843.

[23] I. Reda, A. Shalaby, A. El-Baz et al., "A new NMF-autoencoder based CAD system for early diagnosis of prostate cancer," 2016 IEEE 13th International Symposium on Biomedical Imaging (ISBI), Prague, 2016, pp. 1237-1240.

[24] SJ, Harkema; J, Hillayer; M, Schmidt-Reas; E, Ardolino; SA, Sisto; AL, Behrman, "Locomotor training: as a treatment of spinal cord injury and in the progression of neurological rehabilitation," *Arch Phys Med Rehabil,* vol. 93, no. 9, pp. 1588-97, 2012.

[25] K. H. Zou, S. K. Warfield, A. Bharatha, C. M. C. Tempany, M. R. Kaus, S. J. Haker, W. M. Wells III, F. A. Jolesz, and R. Kikinis, "Statistical validation of image segmentation quality based on a spatial overlap index," *Aca. Radiol.,* vol. 11, no. 2, p. 178–189, 2004.